Thermal Spray 2023: Proceedings from the
International Thermal Spray Conference
May 22—25, 2023; Quebec City, Canada
https://doi.org/10.31399/asm.cp.itsc2023p0414

Check for updates

Copyright © 2023 ASM International®
All rights reserved.
www.asminternational.org

Alloy design of feedstock material for additive manufacturing: exploring the Al-Co-Cr-Fe-Ni-Ti compositionally complex alloys

L. Gerdt[1], M. Müller[1], M. Heidowitzsch[1], J. Kaspar[1], E. Lopez[1], M. Zimmermann[1,2], C. Leyens[1,2], A. Hilhorst[3], P.J. Jacques[3]

1 Fraunhofer Institute for Material and Beam Technology IWS, Dresden, Germany
E-Mail: info@iws.fraunhofer.de, Phone: +49 351 83391-0

2 Technische Universität Dresden, Institute of Materials Science, Germany

3 UCLouvain, Institute of Mechanics, Materials and Civil Engineering (iMMC), IMAP, Place Sainte Barbe 2, Louvain-la-neuve, 1348, Belgium

Abstract

The need for sustainable use of resources requires continuous improvement in the energy efficiency and development of new approaches to the design and processing of suitable materials. The concept of high entropy alloys (HEAs) has recently been extended to more general compositional complex alloys (CCAs) and multi-principal element alloys (MPEAs) [1]. One of the major challenges on the way to application of these alloys is the extensive design and selection efforts due to the great variety of possible compositions and its consequences for workability and resulting material properties. The favorable high-temperature strength of Ni-based and Co-based superalloys is ascribed to a defined γ/γ' structure consisting of a disordered FCC A1 matrix and ordered L_{12} γ' precipitates [2]. In the current work we extended this design concept to CCAs, allowing disordered BCC A2 and ordered B2 phases in additions or in substitution of the original γ/γ' structure. We used a high-throughput screening approach combining CALPHAD-based computational tools with in situ alloying by means of laser cladding. Wall-type specimens with gradient composition in the system Al-Co-Cr-Fe-Ni-Ti with varying Al, Ti and Cr content were analyzed. The combined modelling and experimental screening approach was demonstrated to be a powerful tool for designing new high performance AM-ready feedstock.

Introduction

Concerns about climate changes and sustainable use of natural resources require more and more drastically energy efficiency and new approaches in materials design and processing. In this context, the use of emerging additive manufacturing (AM) methods can enable the processing of advanced materials into complex shapes with large material and cost savings as well as effective recycling strategies. An efficient energy production and storage can only be achieved by the development of new high temperature alloys and AM technologies. Therefore, there is a strong need to develop novel metallic materials, such as HEAs or CCAs, for high-temperature applications with superior mechanical properties as well as oxidation and wear resistance. The conventional solutions, such as Co-base alloys are being phased out due to ecological and health concerns [3].

Although the novel material group of HEAs offers a huge potential for being the next generation high-temperature materials, an industrial application of these alloys faces considerable challenges in design, raw material and feedstock availability and quality, alloy processing as well as improved understanding of the relationship between processing parameters and alloy structure and performance [4,5].
After Cantor et al. introduced CoCrFeMnNi HEA [6] a wide variety of derivate alloy systems were designed and analyzed by numerous research groups. One of such alloy systems is CoCrFeNi with Ti and Al additions, which has shown promising balance between strength and ductility, creep resistance comparable to Nickel-based superalloys, high thermodynamic stability, and good oxidation resistance [7–9]. Furthermore, the high entropy superalloy (HESA) concept has been established to describe alloy systems consisting of FCC matrix and L12 precipitates [10,11]. Precipitation strengthening has been shown to be an effective mechanism to produce alloys with good mechanical properties over a wide range of temperatures. The favorable high-temperature strength of Ni-based and Co-based superalloys can be ascribed to a defined structure consisting of a disordered FCC A1 matrix (γ) and ordered FCC L12 precipitates (γ') [2]. The same approach has been used to design new HESAs for high-temperature applications based on Co-Cr-Fe-Ni as principal elements and alloying additions of Al, Cu, Mo, Nb and Ti. This HESA approach can offer lower density as well as higher phase stability and strength at higher temperatures than Ni-based superalloys [12,13].

In addition to these microstructural criteria, there exist other aspects that should be considered: the sustainability, the economic viability and the processability of alloys. To achieve these goals, Fe and Ni rich alloys are favored with respect to Co and Cr. Due to their chemical complexity, the advances in properties of HEAs are often not sufficient to counterbalance the high material cost compared to conventional alloys in structural applications. However, when used as coating, the increase in cost is not as prohibitive and can be justified by better properties. Up to now, the commercial use of CCAs or HESAs has still not succeeded, mainly due to the lack of availability of the feedstock material and comprehensive qualification of new alloys especially for applications in energy and aerospace sectors. Furthermore, the alloy design in the field

Downloaded from http://dl.asminternational.org/itsc/proceedings-pdf/ITSC2023/84536/414/649496/itsc2023p0414.pdf
by guest

of CCA still remains a time-consuming process. Simulation tools like CALPHAD approach can significantly accelerate this process, by thermodynamically-based calculations of phase constitution within a wide compositional range [14,15]. However, the accuracy of such calculations is dependent on elemental composition and is not always reliable, particularly for complex compositions with six and more components, especially if not all constitutive binary and ternary phase diagrams are fully assessed. In order to consider a large number of systems of interest that potentially meets our design criteria, a first screening was performed using the CALPHAD approach. This approach consists of a description of the equilibrium state of an alloy for given conditions (temperature, pressure, composition) by modeling its Gibbs energy, based on thermodynamic databases. Design rules were established to obtain FCC A1 + FCC L12 type microstructures while avoiding detrimental secondary phases such as σ-phase and allowing to some extent the presence of ordered BCC B2 phase. This microstructure can be achieved by a two-step heat treatment consisting of homogenization and precipitation hardening. The formation of brittle σ-phase in the explored system should be critically considered, especially in the targeted temperature range of 600 °C < T < 800 °C [7,16]. Therefore, an approach with low Cr alloy design has been selected, as Cr in particular is a critical element for σ-phase formation. A compositional field based on CoFeNi system with additions of Al (4 and 10 at. %) and Ti (5 and 6 at.-%) and varying Cr content in the range of 0 to 15 at.-% has been explored by using CALPHAD approach and then validated by means of high-throughput screening by laser cladding, scanning electron microscopy (SEM) analysis and hardness measurements. In particular the effect of Cr content on possible formation of brittle σ-phase was in the scope of the current study.

Experimental Methods

In order to enable a high throughput analysis of the $(CoFeNi)_{1-x-y-z}Ti_xAl_yCr_z$ phase space, specimens with altering Al and Ti contents were fabricated by means of direct energy deposition (DED) with laser as energy source. Figure 1a)-c) shows the experimental DED set-up, described in more detail in an earlier paper[17]. Compositionally graded ~2.5 mm thick wall specimens were printed layer by layer. Chemical composition has been varied successively every few layers by varying feeding rates of pre-alloyed CoFeNi-powder as well as elemental Ti, Al and Cr powders. Accordingly, areas of distinct compositions with sharp transitions within each sample were generated. Thus, microstructure and hardness of the respective compositions has been characterized along the build direction of the samples as shown in Figure 1d, e.

The DED machine utilized was an Arnold Ravensburg type 19389 MTH. By adjusting the rotational speed and hence the feeding rates of three independent GTV PF 2/2 disk powder feeders (GTV Verschleißschutz GmbH, Germany) the amount of each powder could be tuned and consequently the composition of the respective layer modified. Deposition was performed with a COAXshield process head (Fraunhofer IWS, Germany) and a 4-kW diode laser LDF 4000-30 (Laserline GmbH, Germany), Figure 1a. The COAXshield is designed to supply the process with an additional shielding gas ensuring an

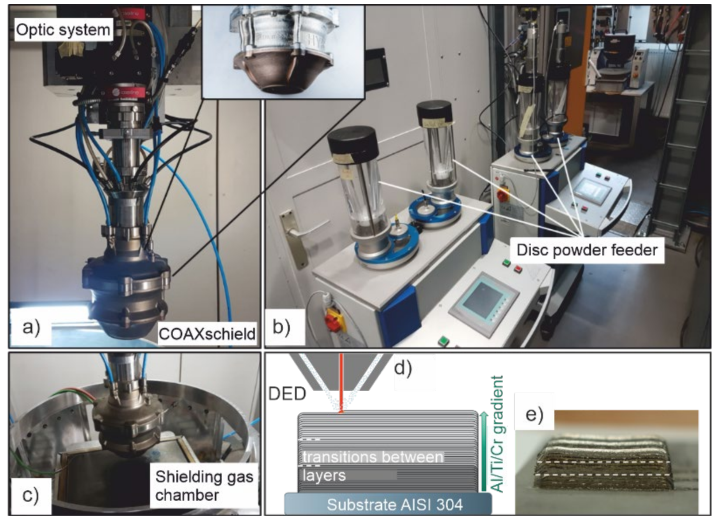

Figure 1: General experimental set-up of DED processing consisting of a) a Laserline optical system with a COAXshield process head, b) four independent disk powder feeders and c) a shielding gas chamber; d) Schematic illustration of the fabrication of graded samples and e) an example of produced wall-type specimen with varying composition

oxygen content within the process zone below 100 ppm. Additionally, the deposition process was carried out in a shielding gas chamber in order to increase safety during the processing of elemental reactive powders such as Ti and Al. 10-mm-thick plates of stainless steel AISI 304 were used as a substrate material. An overview of the targeted and measured compositions within investigated layers is represented in Table 1.

Table 1: Overview of investigated compositions along build-height of manufactured specimens

Sample	Nominal composition (CoFeNi – rest)	Chemical composition by EDS (at.-%)					
		Al	**Ti**	**Cr**	**Fe**	**Co**	**Ni**
V1-01	Al4Ti6Cr0	4.9	8.3	0.1	29.3	28.8	28.6
V1-02	Al4Ti6Cr5	3.9	8.2	4.0	28.0.	28.0	27.8
V1-03	Al4Ti6Cr10	4.4	8.2	9.0	26.0	26.1	26.3
V1-04	Al4Ti6Cr15	4.7	8.6	14.4	24.0	24.1	24.1
V2-01	Al10Ti5Cr0	10.2	6.6	0.2	27.7	27.8	27.4
V2-02	Al10Ti5Cr5	11.3	6.7	4.2	25.9	26.0	25.9
V2-03	Al10Ti5Cr10	11.0	6.5	8.3	24.6	24.9	24.7
V2-04	Al10Ti5Cr15	11.2	6.5	13.4	22.9	23.1	22.8

Table 2 lists the deposition process parameters. For process calibration a customized powder particle sensor was used to measure the three different powder streams. During the deposition process, the different particle streams are first combined in a particle mixing chamber before they are supplied to the coaxial deposition nozzle to achieve a homogeneous mixing of the powders. For further assessment, samples underwent homogenization heat treatment at 1,150 °C for 24 h

Downloaded from http://dl.asminternational.org/itsc/proceedings-pdf/ITSC2023/84536/414/649496/itsc2023p0414.pdf
by guest

(H) and precipitation hardening at 725 °C for 24 h (A) in order to study the evolution of microstructure and mechanical properties.

Table 2: DED process parameters for manufacturing wall-type specimens.

Parameter		Value
Laser power [W]		500
Travel speed [mm/min]		400
Laser spot diameter [mm]		1.6
Shielding and feeding gas		Ar
Powder Mass Rate [g/min]	Al	0.10 – 0.26
	Ti	0.22 – 0.26
	CoFeNi	3.84 – 4.60
	Cr	0.00 – 0.72

The temperatures for solution heat treatment and for precipitation hardening were defined based on the preliminary results of the CALPHAD calculations. All specimens were water quenched. After each processing step, the microstructure of the specimens with different chemical compositions was characterized by means of SEM analysis. For microstructural characterization a scanning electron microscope JEOL JSM-7800F (Jeol, Japan) with energy dispersive spectroscopy (EDS) detector Oxford X-Max (Oxford Instruments, UK) and electron backscattered diffraction (EBSD) detector NordlysNano (Abingdon, UK) were used. Hardness HV0.1 measurements were conducted by utilizing a LECO AMH-43 (LECO, USA). All the thermodynamic calculations were performed using the Thermo-Calc software version 2022a with the TCHEA5 database.

Results and Discussion

The low Cr alloy design aimed at achieving σ-free compositional field with possibly high content of γ'-precipitations within FCC-A1 matrix. Figure 2 shows the CALPHAD calculations for a compositional field $(CoFeNi)_{90-x-y}$ with fixed Cr content of 10 at.-% and varying Al and Ti content ($0 < x,y < 10$ at.-%) representing regions with binary FCC A1 + FCC L12 (γ') microstructure.

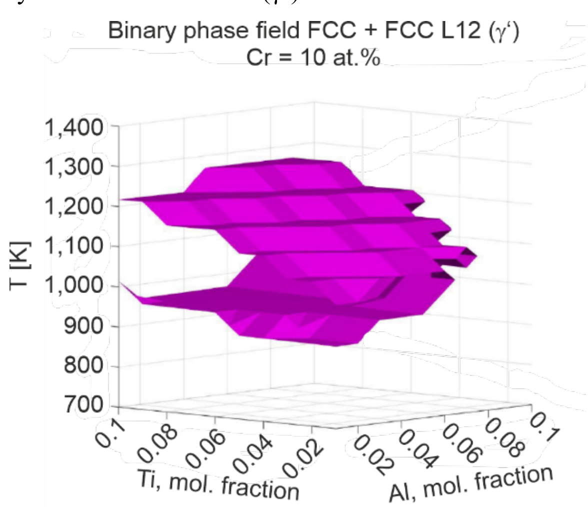

Figure 2: Calculated binary phase field FCC + FCC L12 L12 for a fixed Cr content of X_{Cr} = 10 at.%

According to these calculations, the binary phase region of interest has high stability in a wide compositional range particularly at the temperature range 1,000 K < T < 1,100 K. Thus, the heat treatment temperature for precipitation hardening was set at T = 998 K (725°C). Considering the σ-phase formation in the investigated alloy system, a possible occurrence of this brittle intermetallic phase has been predicted by CALPHAD calculations in the temperature region 770 K < T < 900 K depending on Al and Ti content (see Fig. 8 in appendix). Furthermore, BCC-B2 phase is expected to be present in the microstructure of heat-treated specimens for compositions with higher Al content, which is in accordance with the available literature data for similar alloy systems [18].

Figure 3 shows the distribution of alloying elements in the manufactured wall-type specimens along the build direction. For both specimens, plateaus (about 2 mm in length) with nearly constant Cr content close to the nominal composition of 0, 5, 10 and 15 at.-% can be observed.

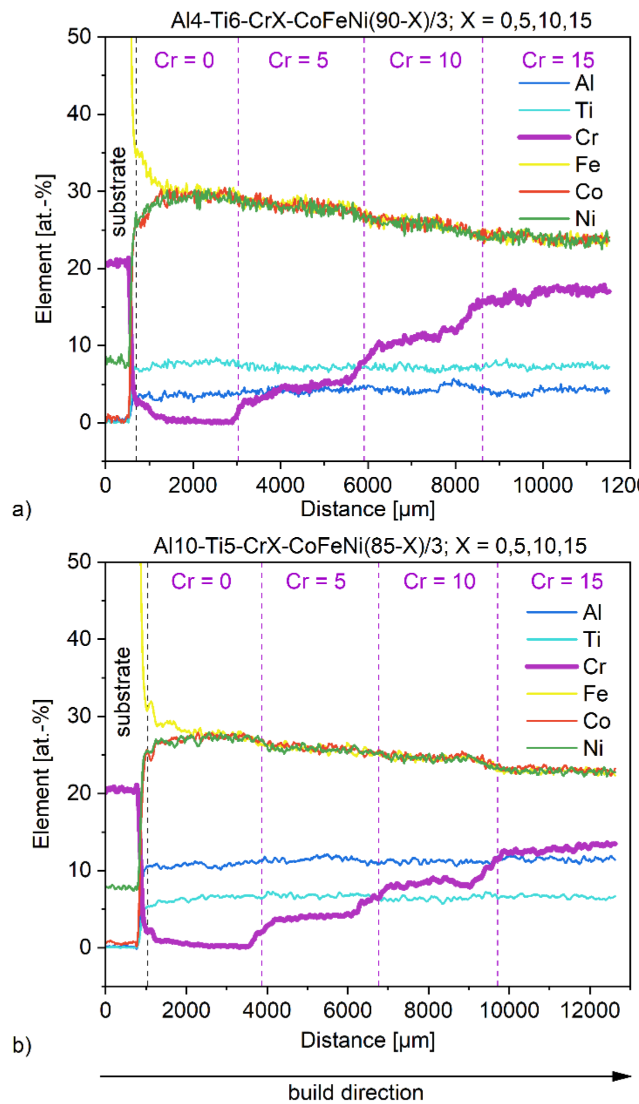

Figure 3: SEM-EDS linescan along the build directions of the wall specimens a) Al4Ti6-system and b) Al10Ti5-system

Downloaded from http://dl.asminternational.org/itsc/proceedings-pdf/ITSC2023/84536/414/649496/itsc2023p0414.pdf by guest

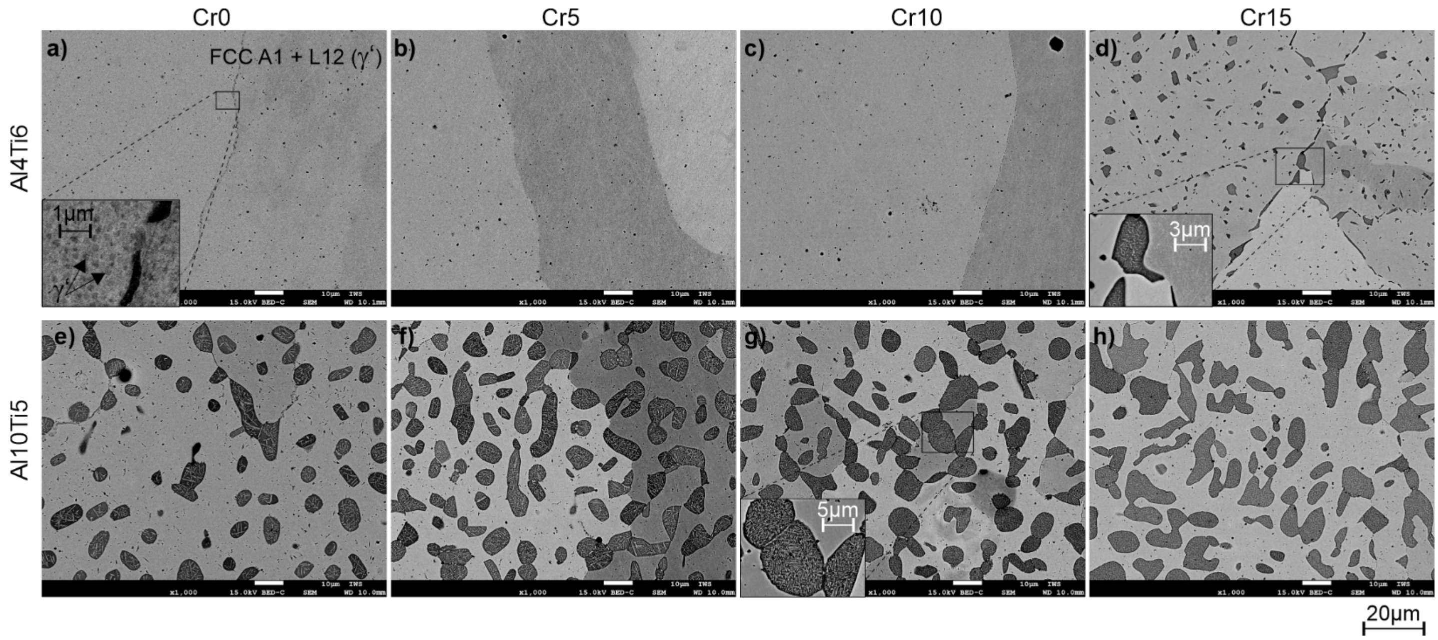

Figure 4: SEM-BSE (back scattered electrons) images of the samples a) Al4Ti6Cr0, b) Al4Ti6Cr5, c) Al4Ti6Cr10, d) Al4Ti6Cr15, e) Al10Ti5Cr0, f) Al10Ti5Cr5, g) Al10Ti5Cr10, h) Al10Ti5Cr15 after two-step heat treatment (H+A).

Figure 4 shows the microstructure analyses by means of SEM providing the first information on phase composition of the investigated system after two-step heat treatment. For the low Al (Al4Ti6) system the microstructure remains purely FCC. Even though at small and intermediate magnifications the nm-sized FCC L12 (γ') precipitation cannot be visualized, the inset in Figure 4a shows exemplarily the dual-phase FCC A1 + FCC L12 (γ') structure until the Cr content reaches X_{Cr} = 15 at.-%. Here the formation of additional BCC phase can be assumed (dark grey regions) based on literature data for similar alloy compositions as well as according to CALPHAD simulations. This can be explained by the simultaneous decrease of Ni and Co content within FCC A1 matrix, which causes this phase's inability to dissolve Al and Ti completely. At higher magnifications, it becomes visible that the particles of BCC phase actually consist of at least two different phases, see inset of Figure 4d). For the system with higher Al content (Al10Ti5) the BCC phase is present in the whole range of Cr content (0-15 at.-%). The phase fraction of BCC phase increased with increasing Cr content. Similar to the low Al system the BCC-phase obviously consists of two different phases. No evidence of the L12 (γ')-precipitates could be found by means of SEM-BSE analysis in Al10Ti5-system independent of Cr content. In order to better understand the nature of phases formed in the investigated systems elemental distribution within these phases has been identified by means of EDS.

Figure 5 shows exemplary EDS-mappings of Ni and Fe for the sample Al4Ti6Cr0. The distribution of these elements provides a further evidence of γ'-formation, which has already been observed by means of SEM-BSE analysis, (Fig. 4a).

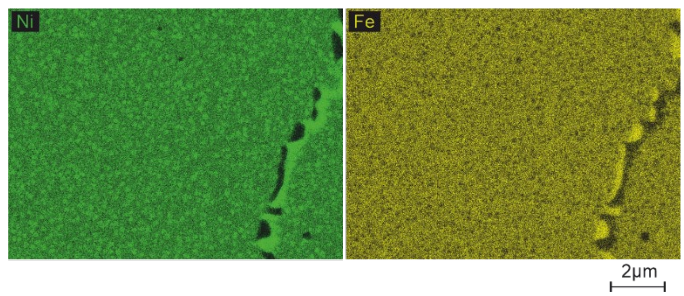

Figure 5: Exemplary SEM-EDS mappings of Ni and Fe for the specimen Al4Ti6Cr0

The γ'-precipitates are Ni- and Al/Ti-rich and have almost zero tolerance for Fe and Cr. The elemental distributions of Al, Ti, Cr and Co are attached as supplementary data in appendix (Figure 8). Figure 6 shows the element distributions for the sample Al10Ti5Cr10. The BCC phase (dark grey regions in Fig. 4g) has higher Al, Ti and Ni contents, compared to the FCC matrix, so that formation of BCC B2 phase can be assumed.

The fine needle-like particles within BCC B2 phase have higher Fe and Cr content. According to the CALPHAD calculations, formation of σ-phase can be expected (please see supplementary data in Fig. 8 in appendix). However, a clear verification of composition and crystallographic structure of these particles was not possible due to their very small size. Regarding the literature data available for similar alloy systems $Al_xCoCrFeNi$ a decomposition of BCC B2 phase into BCC B2 and BCC A2 can be taken into account as a possible mechanism of the second phase formation within BCC B2 structure [18,19].

Downloaded from http://dl.asminternational.org/itsc/proceedings-pdf/ITSC2023/84536/414/649496/itsc2023p0414.pdf
by guest

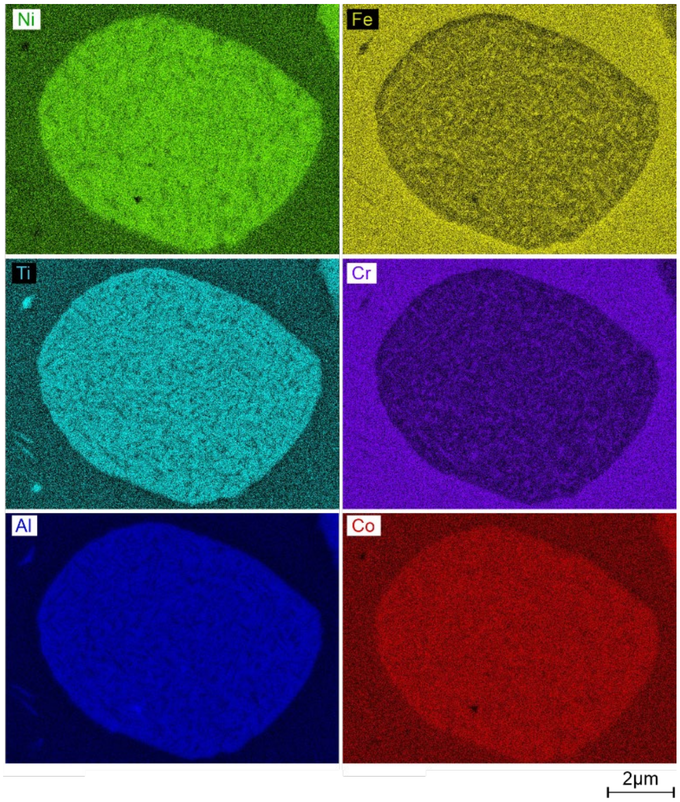

Figure 6: Exemplary SEM-EDS mappings of Ni and Fe for the specimen Al4Ti6Cr0

Here, the BCC A2 phase is also Cr- and Fe-rich, which makes the distinguishing between BCC A2 and σ-phase by means of EDS analysis almost impossible. However, Stryzhyboroda et al. have identified the small particles within the BCC B2 structure as σ-phase by means of EBSD analysis in $Al_{0.7}CoCrFeNi$ alloy after arc melting and subsequent annealing at T = 900 °C for t = 24 h followed by water quenching [19]. The precise phase verification in our present study will be within the scope of further investigations.

The effect of two-step heat treatment on microstructural evolution of the investigated alloys resulted in significant changes of the alloys hardness. The hardness HV0.1 linescans along the build direction of the specimens are represented in Figure 7. In as built (AB) condition a similar trend can be observed for all specimen series. The hardness of the investigated system increases with increasing Ti and Al content from about 320 HV0.1 for Al4Ti6-system to > 350 HV for Al10Ti5-system. This can be explained by the presence of the hard BCC B2 phase in the latter one. The effect of Cr content is less pronounced and becomes considerable only at Cr content X_{Cr} >10 at.-% for Al10Ti5-system. A significant strengthening of the microstructure after precipitation hardening can be observed in both systems. The hardness increased by approximately 100 HV0.1 in Al4Ti6-system in the whole range of Cr content. Here, the formation of the L12 (γ')-precipitates, which can be observed in Figure 4a), is the main strengthening mechanism. For Al10Ti5-system no evidence of L12 (γ') formation can be verified by means of SEM analysis, however, the increase of hardness, especially at lower Cr content X_{Cr} < 10 at.-% indirectly indicates a possible precipitation hardening effect in the microstructure.

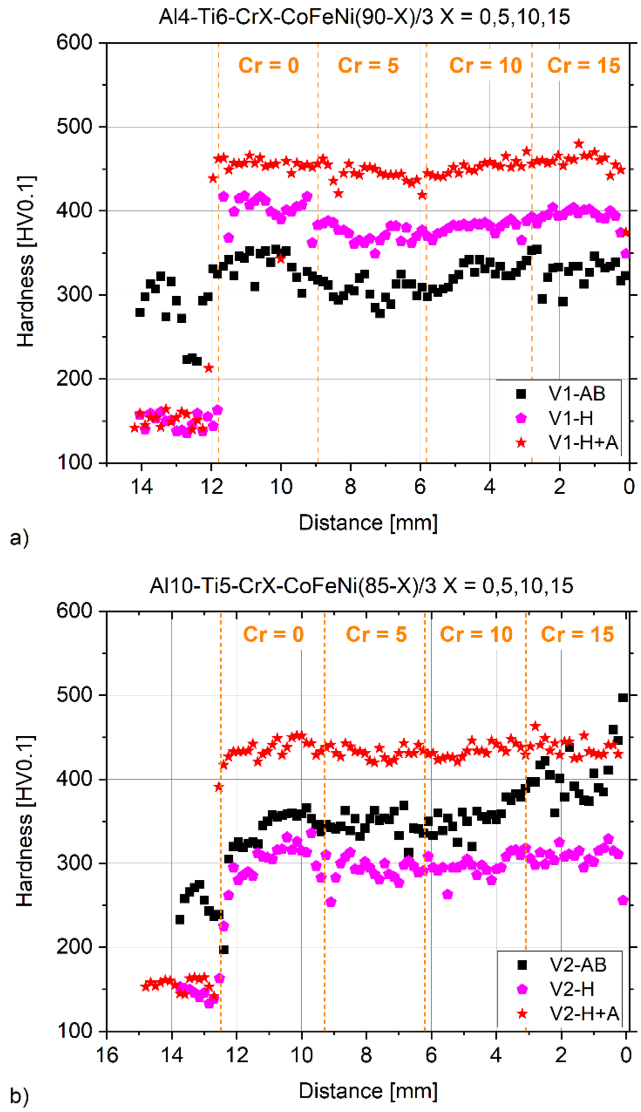

Figure 7: Hardness line scans along the build direction of the samples with varying Cr content after laser cladding (AB – as built), homogenization heat treatment (H) and age hardening (H+A) for a) Al4Ti6-system b) Al10Ti5-system

For Al- and Cr-rich compositions, the impact of BCC-B2 with fine needle-like particles of the third phase on the mean hardness becomes more pronounced, so that the effect of heat treatment is getting less pronounced.

Interestingly, the investigated alloy systems showed different response to homogenization heat treatment. For Al4Ti6 it resulted in hardness increase compared to as built condition. However, a slight decrease of the hardness has been observed in the Al-rich system. For the second one the altering morphology and distribution of the BCC phase is a possible reason for the hardness decrease, as the BCC particles became coarser. In Al4Ti6-system which remains single phase in the whole composition range in AB condition and after homogenization heat treatment, a stronger impact of solid solution strengthening can be assumed, as all alloying elements are dissolved in the FCC A1 structure. Here, the dissolution of element segregations, in particular Ti, can be considered as a possible mechanism causing an increase of the hardness after

Downloaded from http://dl.asminternational.org/itsc/proceedings-pdf/ITSC2023/84536/414/649496/itsc2023p0414.pdf
by guest

homogenization heat treatment (for evidence please see Fig. 11 in appendix).

Conclusions

In the present work different compositions in the $(CoFeNi)_{1-x-y-z}Ti_xAl_yCr_z$ CCAs system have been synthesized by a laser-based DED process and thoroughly investigated regarding the microstructure and hardness evolution during a two-step heat treatment. Based on the results the following conclusions can be drawn:

- The alloy system with low Al- and Ti-content (Al4Ti6) exhibits single phase FCC structure (FCC-A1) in a large range of Cr-content. By increasing Cr content $X_{Cr} > 10$ at.% the formation of BCC B2 phase and possibly σ-phase occur after homogenization and annealing. Furthermore, precipitation of FCC-L12 (γ') within FCC-A1 could be confirmed by means of SEM and -EDS analysis. This resulted in a significant age hardening response, i.e. an increase of the microhardness during age hardening of Al4Ti6.
- For Al-rich Al10Ti5 alloy system a more complex phase composition has been observed. The microstructure consisted of FCC (FCC-A1) and BCC (BCC-B2) phases with small needle-like particles of the third phase within BCC structure. According to the EDX analysis as well as considering the CALPHAD calculations and literature data, formation of BCC-A2 or σ-phase can be assumed. The exact nature of this third phase has to be further investigated. Although no evidence of γ'-precipitates was provided by SEM analysis in this system, the hardness of the explored alloys has been significantly increased by two-step HT.

Considering the achieved level of microhardness values of about 450 HV0.1, both alloy systems show promising properties for applications under mechanical loading conditions. This should also be reflected by by tensile testing planned in the future. Furthermore, the nature of the fine needle-like particles in the BCC-B2 structure has to be verified by means of high-resolution TEM analysis.

Acknowledgement

The presented results are part of the project "Novel metallic materials, feedstock and fabrication processes for high-performance additive manufactured goods (NovMat-AM: proposal number 100582943)". This project is co-financed with tax funds on the basis of the budget adopted by the Saxon Parliament. The authors wish to express special thanks to our colleague Andrea Ostwaldt for metallographic sample preparation and light microscopy analysis of the investigated samples.

References

[1] D. B. Miracle, O. N. Senkov, *Acta Materialia* **2017**, *122*, 448.
[2] D. Hausmann, C. Solís, L. P. Freund, N. Volz, A. Heinemann, M. Göken, R. Gilles, S. Neumeier, *metals* **2020**, *10*, 321.
[3] P. Novák, T. Bellezze, M. Cabibbo, E. Gamsjäger, M. Wiessner, D. Rajnovic, L. Jaworska, P. Hanus, A. Shishkin, G. Goel, S. Goel, *Materials (Basel, Switzerland)* **2021**, *14*.
[4] M. Baker, *Defining Pathways for Realizing the Revolutionary Potential of High Entropy Alloys: A TMS Accelerator Study*, The Minerals, Metals & Materials Society **2021**.
[5] J. Bishop-Moser, D. Miracle, *MFORSIGHT* **2018**.
[6] B. Cantor, I. Chang, P. Knight, A. Vincent, *Materials Science and Engineering A* **2004**, *375-377*, 213.
[7] L. Moravcikova-Gouvea, I. Moravcik, M. Omasta, J. Veselý, J. Cizek, P. Minárik, J. Cupera, A. Záděra, V. Jan, I. Dlouhy, *Materials Characterization* **2020**, *159*, 110046.
[8] Y.-J. Chang, A.-C. Yeh, *Journal of Alloys and Compounds* **2015**, *653*, 379.
[9] M.-H. Chuang, M.-H. Tsai, W.-R. Wang, S.-J. Lin, J.-W. Yeh, *Acta Materialia* **2011**, *59*, 6308.
[10] J. Joseph, M. Senadeera, Q. Chao, K. F. Shamlaye, S. Rana, S. Gupta, S. Venkatesh, P. Hodgson, M. Barnett, D. Fabijanic, *Journal of Alloys and Compounds* **2021**, *888*, 161496.
[11] H. M. Daoud, A. M. Manzoni, N. Wanderka, U. Glatzel, *JOM* **2015**, *67*, 2271.
[12] T. Yang, Y. Zhao, W. Liu, J. Kai, C. Liu, *J. Mater. Res.* **2018**, *33*, 2983.
[13] T.-K. Tsao, A.-C. Yeh, C.-M. Kuo, H. Murakami, *Adv Eng Mater* **2017**, *19*, 1600475.
[14] Y. Li, B. Holmedal, B. Liu, H. Li, L. Zhuang, J. Zhang, Q. Du, J. Xie, *Calphad* **2021**, *72*, 102231.
[15] P. L. Conway, T. Klaver, J. Steggo, E. Ghassemali, *Materials Science and Engineering: A* **2022**, *830*, 142297.
[16] X. Zuo, A. Miotti Bettanini, A. Hilhorst, P. J. Jacques, N. Moelans, *J. Phase Equilib. Diffus.* **2021**, *42*, 794.
[17] M. Müller, C. C. Labisch, L. Gerdt, L. Bach, M. Riede, J. Kaspar, E. López, F. Brueckner, M. Zimmermann, C. Leyens, *Journal of laser applications* **2023**, *35*, 12006.
[18] U. Hecht, S. Gein, O. Stryzhyboroda, E. Eshed, S. Osovski, *Front. Mater.* **2020**, *7*, 238.
[19] O. Stryzhyboroda, V. T. Witusiewicz, S. Gein, D. Röhrens, U. Hecht, *Front. Mater.* **2020**, *7*, 238.

Downloaded from http://dl.asminternational.org/itsc/proceedings-pdf/ITSC2023/84536/414/649496/itsc2023p0414.pdf
by guest

Appendix

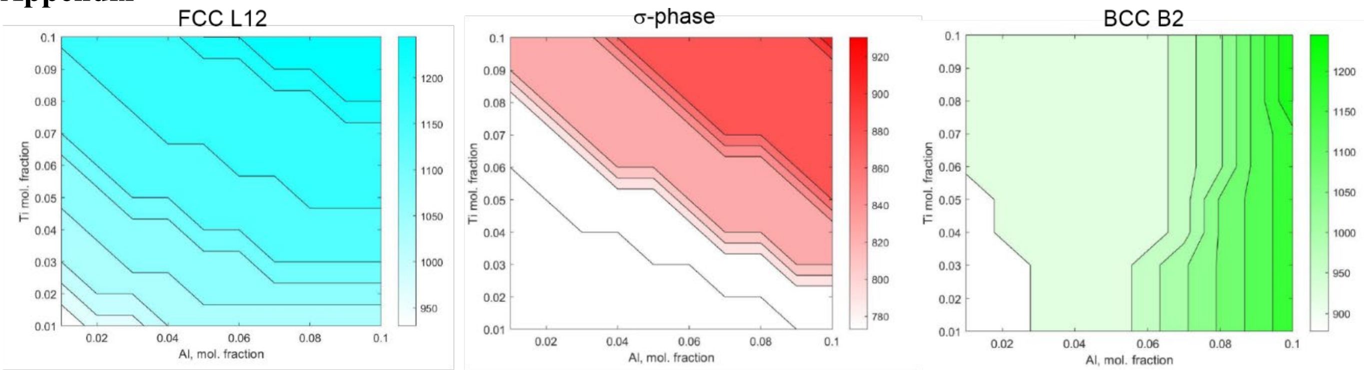

Figure 8: Solvus isosurfaces (temperature below which the corresponding phase met the condition > 1 mol.%) for FCC L12, σ-phase and BCC-B2 for a fixed Cr content of X_{Cr} = 10 at.%

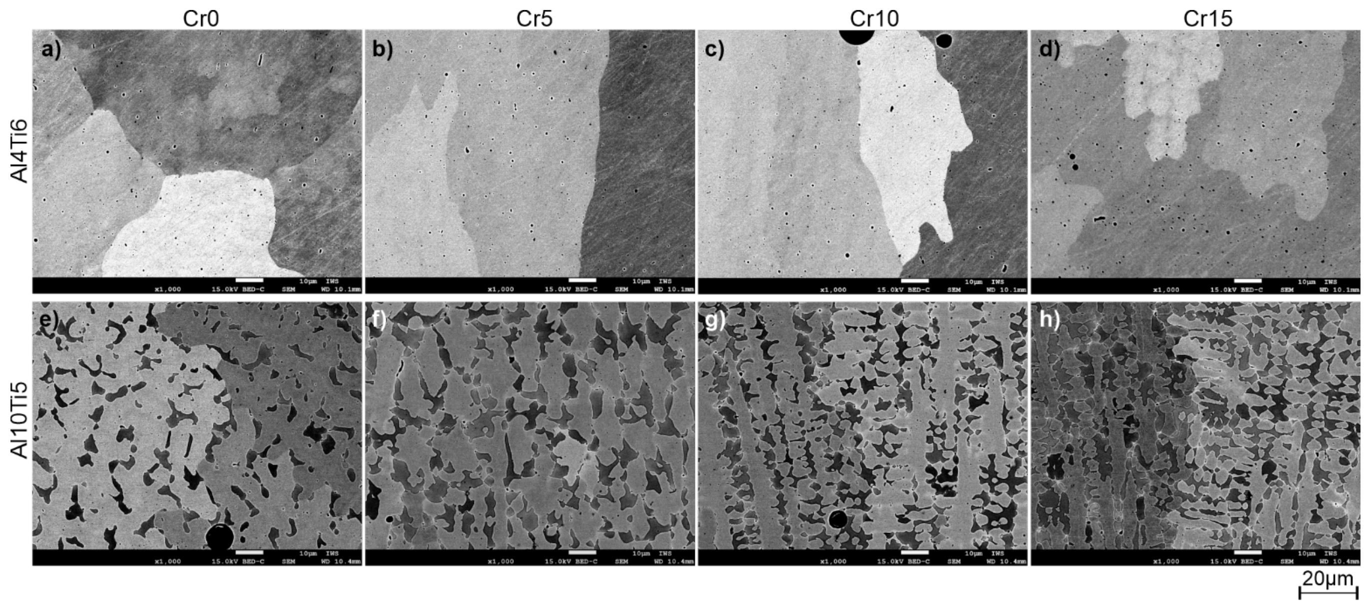

Figure 9: SEM-BSE (back scattered electrons) images of the samples a) Al4Ti6Cr0, b) Al4Ti6Cr5, c) Al4Ti6Cr10, d) Al4Ti6Cr15, e) Al10Ti5Cr0, f) Al10Ti5Cr5, g) Al10Ti5Cr10, h) Al10Ti5Cr15 after laser cladding (AB)

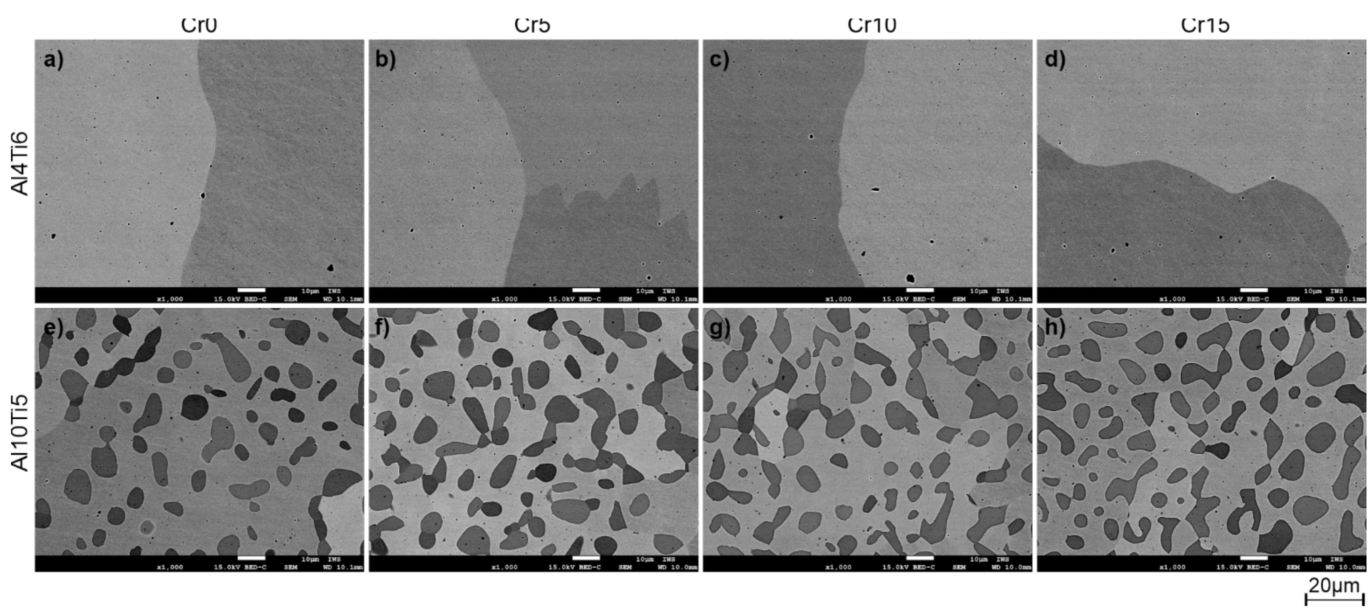

Figure 10: SEM-BSE (back scattered electrons) images of the samples a) Al4Ti6Cr0, b) Al4Ti6Cr5, c) Al4Ti6Cr10, d) Al4Ti6Cr15, e) Al10Ti5Cr0, f) Al10Ti5Cr5, g) Al10Ti5Cr10, h) Al10Ti5Cr15 after homogenization heat treatment (H)

Downloaded from http://dl.asminternational.org/itsc/proceedings-pdf/ITSC2023/84536/414/649496/itsc2023p0414.pdf
by guest

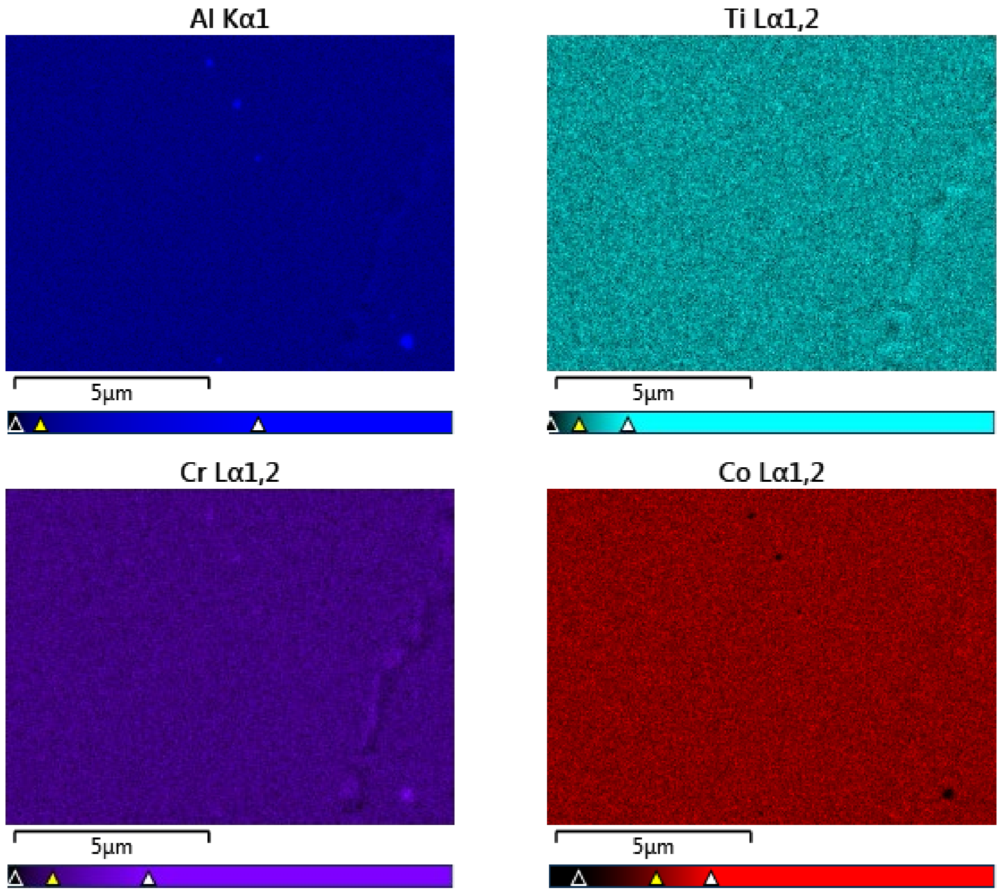

Figure 8: SEM-EDS mappings of Al, Ti, Cr and Co for the specimen Al4Ti6Cr0 after two-step heat treatment

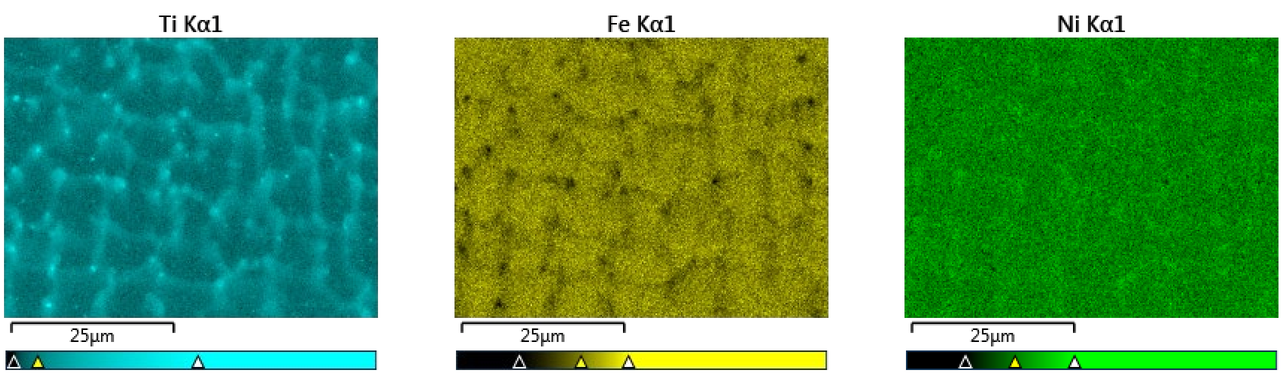

Figure 9: exemplary SEM-EDS mappings of Ti, Fe and Ni for the specimen Al4Ti6Cr0 in as built condition

Downloaded from http://dl.asminternational.org/itsc/proceedings-pdf/ITSC2023/84536/414/649496/itsc2023p0414.pdf
by guest